Capacitance-voltage characteristics of a Schottky junction containing SiGe/Si quantum wells

Fang Lu, Dawei Gong, Jianbao Wang, Qinhua Wang, Henghui Sun, and Xun Wang
Fudan T. D. Lee Physics Laboratory and Surface Physics Laboratory, Fudan University, Shanghai 200433, China
(Received 21 March 1995)

The capacitance-voltage (C-V) characteristics of SiGe/Si quantum wells located near or in the space-charge region of a Schottky barrier have been numerically simulated by solving the Poisson equation. A physical picture of the variations of energy band and charge density in the quantum-well structure under the bias voltage is presented. The predominant feature of the C-V curves of quantum-well structures is the appearance of a capacitance plateau for single quantum wells or a series of plateaus for multiple-quantum-well samples. From the coincidence between the measured C-V curve and the simulated one, the band offset at the heterointerface could be derived. Moreover, the structural parameters of the quantum-well sample could be obtained from the measured C-V curves. It is found that the carrier-concentration profile derived from the C-V curve by the ordinary differential method does not coincide with the real carrier distribution in the quantum well; only the peak height of the C-V carrier concentration profile is related to the average carrier concentration in the well.

I. INTRODUCTION

Capacitance-voltage (C-V) technique is a traditional method in measuring the carrier-concentration profile of semiconductor bulk materials. In extensive studies of semiconductor heterojunctions and quantum wells, attempts have been made by using the C-V method to measure the carrier-concentration profile in the heterostructures. However, due to the limitation of the depth resolution by the Debye length, the carrier-concentration profile obtained by the C-V measurement (known as the C-V carrier-concentration profile[1]) is found to be different from the real concentration in a heterostructure.[2,3] Kroemer *et al.*[2] suggested that although the C-V carrier-concentration profile does not represent the real carrier distribution, it can be used to derive the band offset at the heterointerface. This approach has been successfully employed in III-V heterojunctions[4] and $Si_{1-x}Ge_x/Si$ double heterojunctions with small Ge compositions ($x<0.14$) in the alloy layers.[5] In the case of quantum-well samples, Letartre, Stievenard, and Barbier[6,7] calculated the C-V characteristics of a $GaAs/In_xGa_{1-x}As/GaAs$ single quantum well located in a depletion region by solving the Poisson equation with the Fermi-Dirac statistics of the two-dimensional electron gas in the well. The information they obtained is still the band offset. In this work, we present a detailed theoretical analysis of the C-V characteristics of a $Si/Si_{1-x}Ge_x/Si$ single quantum well contained in the depletion region of a Schottky barrier, revealing cogently the physical pictures of the variations of energy band and the extension of space-charge regions under different bias voltages. The experimental results coincide well with the theoretical prediction. In addition to the band offset which could be obtained from the numerical simulation of C-V curves, the structural parameters of the quantum well could also be derived from the measured C-V curves. The theoretical study of the C-V characteristics of SiGe/Si multiple quantum wells has also been carried out, and the coincidence with the experiments is verified.

II. VOLTAGE DEPENDENCE OF ENERGY BAND OF A SCHOTTKY BARRIER CONTAINING A SINGLE QUANTUM WELL

If there is a quantum well with the well width of L_w and barrier thickness of L_b in the space-charge region of a Schottky barrier, the potential distribution $V(x)$ in the sample fulfills the following Poisson equation:

$$\frac{d^2V}{dx^2}=-\frac{\rho(x)}{\varepsilon}, \tag{1}$$

where ε is the dielectric constant, and $\rho(x)$ is the charge density that could be expressed as

$$\rho(x)=q[p(x)-N_{\mathrm{Ab}}^{-}(x)], \tag{2}$$

and

$$\rho(x)=q[p(x)-N_{\mathrm{AW}}^{-}(x)], \tag{3}$$

in the barrier and well regions, respectively. q is the electric charge, and $p(x)$ is the hole concentration. $N_{\mathrm{Ab}}^{-}(x)$ and $N_{\mathrm{AW}}^{-}(x)$ are the ionized acceptor concentration in the barrier and well regions, respectively. $N_{\mathrm{AW}}^{-}(x)$ is related to the Fermi level E_F by the following expression:

$$N_{\mathrm{AW}}^{-}=N_{\mathrm{AW}}(x)\frac{1}{2\ \exp\left(\dfrac{E_{\mathrm{vw}}+\Delta E_a-E_f}{kT}\right)+1}, \tag{4}$$

where E_{vw} is the top of the valence band in the well, ΔE_a is the ionization energy of acceptors, $N_{\mathrm{Aw}}(x)$ is the doping concentration in the well, and k is the Boltzmann constant. The hole concentration in the well could be expressed by either a three-dimensional formula for a wide well,[8] or a two-dimensional one for a narrow well,[9] i.e.,

$$p_{w3}=N_{\mathrm{vw}}\exp[-(E_F-E_{\mathrm{vw}})/kT], \tag{5}$$

where N_{vw} is the effective density of states in the valence band, or

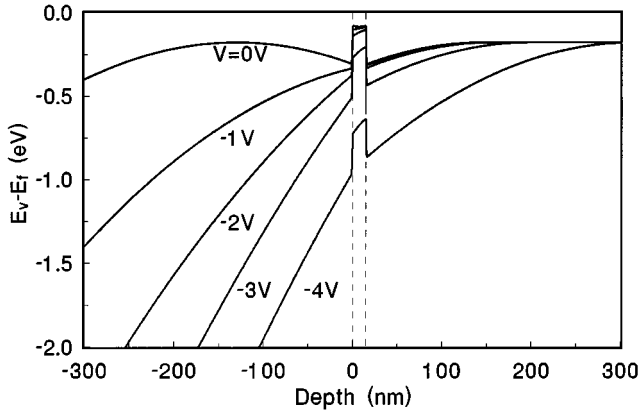

FIG. 1. Variation of the valence band of a single quantum well under different voltages.

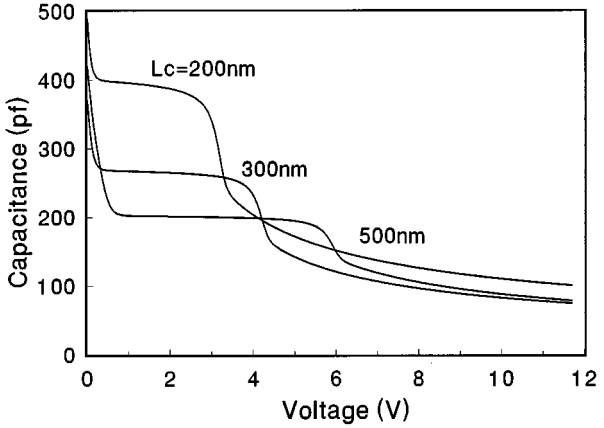

FIG. 2. The calculated C-V curves with different thicknesses of cap layers.

$$p_{w2}=2\frac{g}{L_W}\left[\sum_{i=1}^{n} i\int_{E_i}^{E_{i+1}} f(E)dE+n\int_{E_n}^{E_{Vb}} f(E)dE\right], \quad (6)$$

where $g=m^*/2\pi h^2$ is the two-dimensional density of states in the K space, m^* is the effective mass of two-dimensional holes in the SiGe well, E_i is the energy of the ith sublevel in the well, E_{vb} is the top of valence band in the barrier, and $f(E)$ is the Fermi distribution function

$$f(E)=1/[1+\exp(E_F-E)/kT]. \quad (7)$$

The first integration in Eq. (6) could be written as

$$\int_{E_i}^{E_{i+1}} f(E)dE=h(E_{i+1})-h(E_i), \quad (8)$$

where $h(E_i)=kT[\ln(1+e^{u_i})-u_i]$, and $u_i=(E_F-E_i)/kT$. Equation (6) thus could be simplified to

$$p_{w2}=(m^*kT/\pi h^2 Lw)\left[nh(E_{vb})-\sum_{i=1}^{n} h(E_i)\right]. \quad (9)$$

By using the boundary conditions of potential and electrical field at the interfaces of well and barrier, the potential distribution and thus the energy band in the whole space-charge region could be calculated numerically. In the calculation, the sublevels in the quantum well were derived by using a model of finite square well. Figure 1 shows the valence band of a single quantum well under different reverse bias voltages. The surface Schottky barrier height of an Al/p-Si contact is taken to be 0.35 eV, as determined from our I-V measurement. The width and Ge content of $\mathrm{Si}_{1-x}\mathrm{Ge}_x$ well are $L_w=15$ nm and $x=0.33$ respectively. The thickness of the Si cap is 300 nm. The valence-band offset $\Delta E_V=0.22$ eV. The doping concentrations in the well and barrier are $N_{\mathrm{Aw}}=4\times10^{17}$ cm^{-3} and $N_{\mathrm{Ab}}=1\times10^{16}$ cm^{-3}, respectively, and the temperature $T=300$ K. Under zero bias, the transfer of holes from the barrier into the well results in the band bending of barrier regions at the two sides of the quantum well, and the depletion region of the Schottky barrier formed by a metal electrode on the top of the Si cap extends basically within the cap layer. Under small bias voltages, the high carrier concentration in the well screens the change of applied electric field, the depletion region is basically limited within the cap and the well layer, and the energy band at the right side of the well changes slightly. After the depletion of the carriers in the well layer under higher bias voltages, the depletion region is then extended over the right side of the quantum well and behaves like an ordinary Schottky barrier.

III. C-V CHARACTERISTICS OF QUANTUM-WELL STRUCTURES

After obtaining the potential and electric-field distribution in the quantum-well structure, we can calculate the charge density Q in the sample under different applied voltages. The C-V curves derived from differentiating the Q-V relations are shown in Fig. 2, where the thicknesses of cap layers are 200, 300, and 500 nm, respectively, while other parameters for the quantum-well structures are the same as those in Fig. 1.

The C-V curves shown in Fig. 2 are quite different to that of a bulk semiconductor. In the samples described above, the total applied ac voltage drops across the cap, the quantum well and the Si substrate (or buffer layer), i.e., $dV=dV_c+dV_w+dV_b$. The overall capacitance C is thus the series of the cap capacitance C_c, the well capacitance C_w, and the buffer capacitance C_b, as expressed by

$$\frac{1}{C}=\frac{dV_c}{dQ}+\frac{dV_w}{dQ}+\frac{dV_b}{dQ}=\frac{1}{C_c}+\frac{1}{C_w}+\frac{1}{C_b}. \quad (10)$$

The values of dV_c, dV_w, and dV_b at different bias voltages can be obtained from the calculation of electric potential profile in the quantum-well structure, thus C_c, C_w, and C_b can be obtained. At low bias voltages, the space-charge region of the Schottky barrier expands basically in the cap layer. The applied ac voltage dV drops across the cap, i.e., $dV=dV_c$ and $dV_w=dV_b=0$. The total capacitance follows the formula of an ordinary Schottky barrier,

$$C_a=A[q\varepsilon N_A/2V]^{1/2}, \quad (11)$$

where A is the area of the electrode. For a sample with a 500-nm cap layer, the result of formula (11) is shown as the dotted curve in Fig. 3. The carrier concentration in the cap

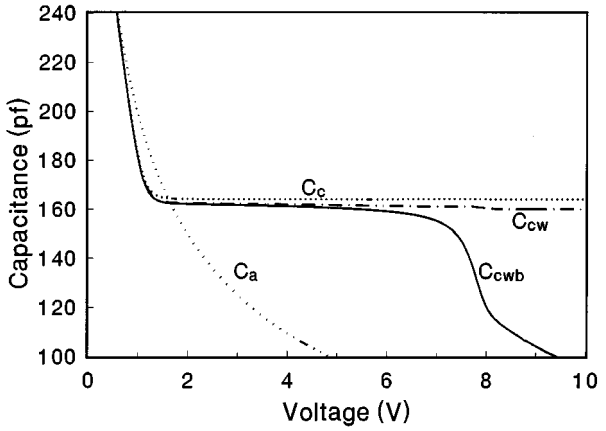

FIG. 3. The calculation results of C_a, C_c, C_{cw}, and C_{cwb} vs voltage.

layer (except in the depletion region near the well boundary) could be determined by the relations

$$x = A\frac{\varepsilon}{C}, \tag{12}$$

$$p(x) = \frac{C^3}{q\varepsilon A\dfrac{dC}{dV}}. \tag{13}$$

With increasing bias voltage, the Schottky barrier begins to overlap with the barrier at the well boundary, and dVw increases accordingly. C_c no longer obeys Eq. (11), as shown in Fig. 3. When the Schottky barrier extends to the well boundary, C_c reaches a constant,

$$C_c' = A\frac{\varepsilon}{L_c}, \tag{14}$$

where L_c is the thickness of the cap. The total capacitance is the series of C_c and C_w,

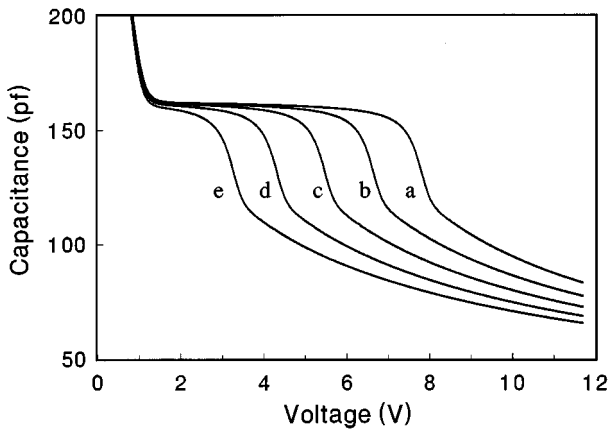

FIG. 4. The calculated C-V curves with different doping concentrations in the well: (a) 4×10^{17} cm^{-3}, (b) 3×10^{17} cm^{-3}, (c) 2×10^{17} cm^{-3}, (d) 1×10^{17} cm^{-3}, and (e) 1×10^{16} cm^{-3}.

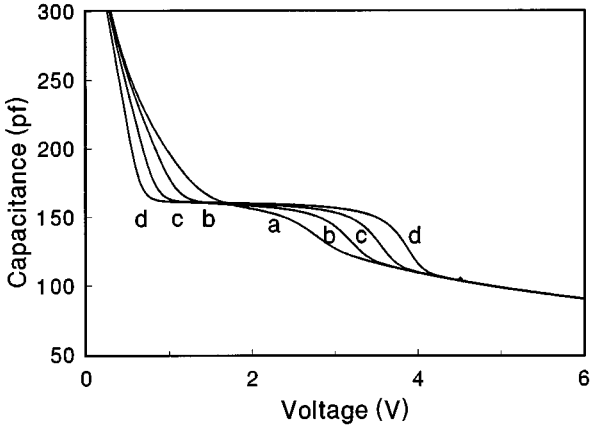

FIG. 5. The calculated C-V curves with different well depths: (a) 0.1 eV, (b) 0.2 eV, (c) 0.3 eV, and (d) 0.4 eV.

$$C_{cw} = \frac{C_c C_w}{C_c + C_w}. \tag{15}$$

In Fig. 3, the dashed curve shows that, near the first inflection point, C_c differs not very much from C_{cw}. C_w is caused by the variation of carrier concentration in the well with the ac voltage. Since the carrier concentration in the well follows an exponential relation with the voltage, C_w is a large capacitance before the depletion of holes in the well. C_{cw} is thus basically determined by C_c. If the carriers in the well are fully depleted by increasing bias voltage, C_w approaches a constant C_w', which is determined by the well width L_w,

$$C_w' = A\frac{\varepsilon_w}{L_w}, \tag{16}$$

where ε_w is the dielectric constant of the $Si_{1-x}Ge_x$ well material,

$$C_{cw}' = \frac{C_c' C_w'}{C_c' + C_w'}. \tag{17}$$

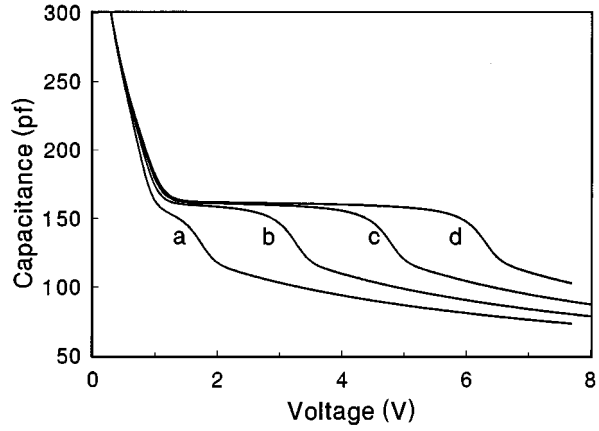

FIG. 6. The calculated C-V curves with different interfacial charge densities: (a) 1×10^{11} cm^{-2}, (b) 0, (c) -1×10^{11} cm^{-2}, and (d) -2×10^{11} cm^{-2}.

TABLE I. Structural parameters of the samples.

No.	Ge content x	Cap width (nm)	Well width (nm)	Barrier width (nm)	No. of periods	Band offset (eV)
A	0.33	200	15		1	0.22
B	0.33	300	15		1	0.22
C	0.40	300	15		1	0.24
D	0.45	300	15		1	0.28
E	0.33	200	15	30	10	0.22
F	0.33	300	5	30	5	0.22

In Fig. 3, C_c' corresponds to the capacitance value where a plateau in the *C-V* curve occurs, from which the thickness of the cap layer and also the location of quantum well could be determined according to Eq. (14). The thicker the cap, the smaller the C_c' and the deviation between C_c' and C_{cw}'; and thus the more accurate the calculation of L_c.

Beyond the plateau in the *C-V* curve, the capacitance decreases again as the bias voltage increases. This is caused by the extension of space-charge region over the buffer layer. C_b is not negligible, and the total capacitance is

$$C_{CWb}=\frac{C_{CW}C_b}{C_{CW}+C_b}. \tag{18}$$

The space-charge region of the buffer expands further with the increase of bias voltage. Beyond a certain voltage, the *C-V* curve is the same as that of the bulk material, from which the carrier concentration in the buffer layer (except near the well boundary) could be determined by Eqs. (12) and (13).

From the above analysis, the basic feature of the *C-V* characteristics of a quantum well which differs from that of a bulk material is the appearance of a capacitance plateau. The capacitance-voltage interval of the plateau are related to the parameters of the quantum well. The capacitance at the first inflection point is determined by the cap thickness, as mentioned above, while the plateau width is determined by many factors, including the thickness and doping concentration of the cap, the doping concentration in the well, and the well depth. For a given thickness ($L_c=500$ nm) and a doping concentration of the cap layer, the *C-V* curves varied with the doping concentration in the well and with the well depth are shown in Figs. 4 and 5.

In addition to the above factors, the *C-V* characteristics may also be influenced by the interfacial charges at the well boundaries. Figure 6 shows the calculated *C-V* curves for a single quantum well with different interfacial charge densities. All other parameters are the same as in Fig. 2. The plateau width increases as the interfacial charge density becomes more negative.

The appearance of a capacitance plateau is caused by the high carrier concentration in the well. A voltage increment is required to deplete the carriers, while the space-charge region does not extend very much. This implies that the ordinary method to determine the carrier-concentration profile by using Eq. (13) is not valid for a quantum-well sample. The fact that the *C-V* carrier concentration profile does not coincide with the real carrier concentration in the well region is due mainly to the above reason. Moreover, since the well width is comparable to or even smaller than the Debye length, the depth profile of the carrier concentration in a quantum well seems meaningless, while the average carrier concentration in the well derived by capacitance plateau is acceptable.

The above analysis is applied to a single quantum well. For the multiple-quantum-well sample, a similar analysis is applicable. The sequential depletion of carriers in individual wells with the increase of bias voltage results in a series of

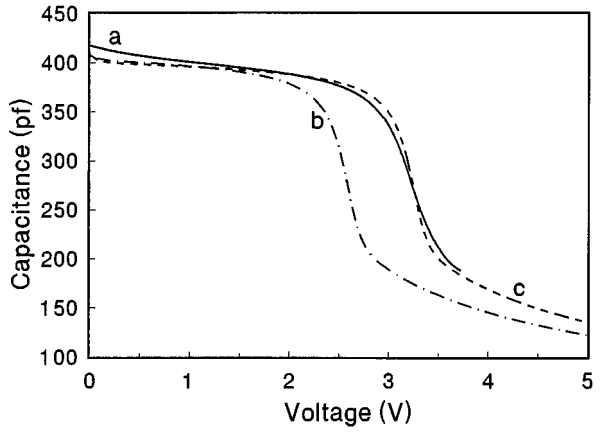

FIG. 7. The measured (a) and simulated (b) and (c) *C-V* curves for sample *A*.

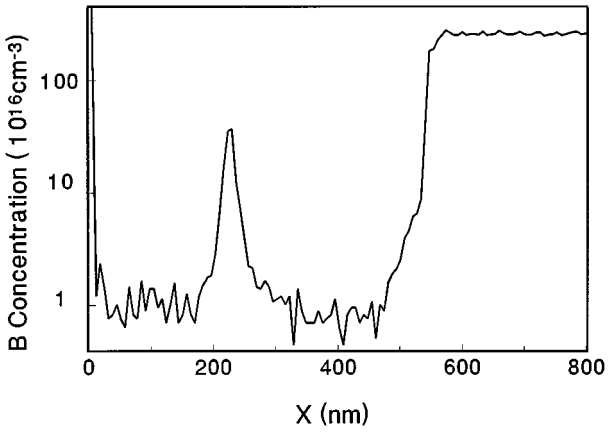

FIG. 8. The B concentration depth profile of sample *A* measured by SIMS.

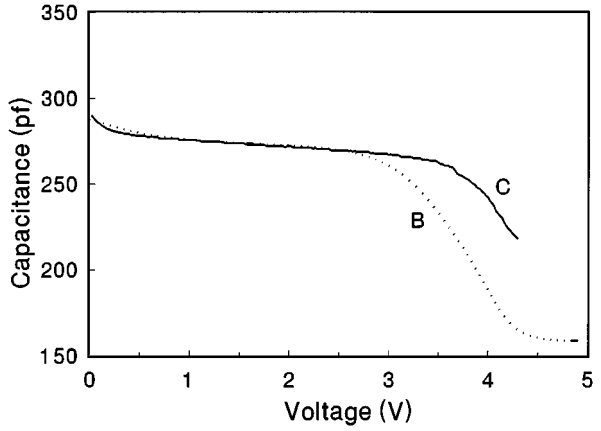

FIG. 9. The measured *C-V* curves of sample *B* and *C*.

capacitance plateaus. We will discuss the *C-V* characteristics of multiple quantum wells in detail below.

IV. SAMPLES AND MEASUREMENTS

The samples were grown on *p*-type Si(100) substrates by molecular-beam epitaxy at a temperature of 500 °C. Before growing quantum wells, a Si buffer layer with a thickness of about 200–300 nm was deposited. The structural parameters of single quantum wells and multiple quantum wells are listed in Table I. The thicknesses and Ge contents were controlled by the deposition rates and monitored by two quartz-thickness monitors. The unintentional doped epitaxial layers were found to be *p* type. A Si cap layer with a thickness of about 200–300 nm was deposited onto the top of the samples. An Ohmic contact was made by evaporating Al onto the backside of the wafer followed by alloying at 500 °C in N_2 ambient. The Schottky contact was made on the front side of the sample by evaporating the Al electrode without alloying. The *C-V* measurements were carried out by using a HP 4275A capacitance meter controlled by an IBM-PC Computer.

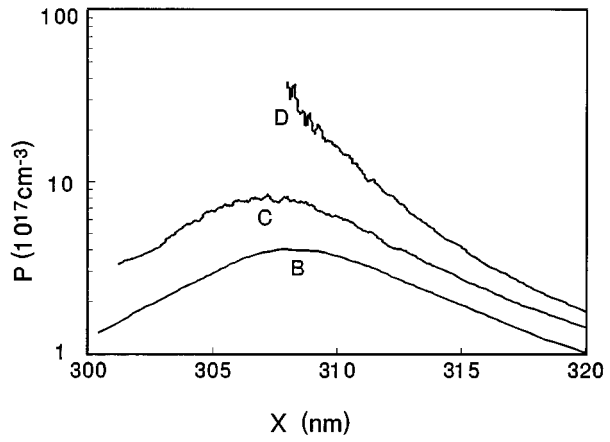

FIG. 10. The *C-V* carrier-concentration profiles of samples *B*, *C*, and *D*.

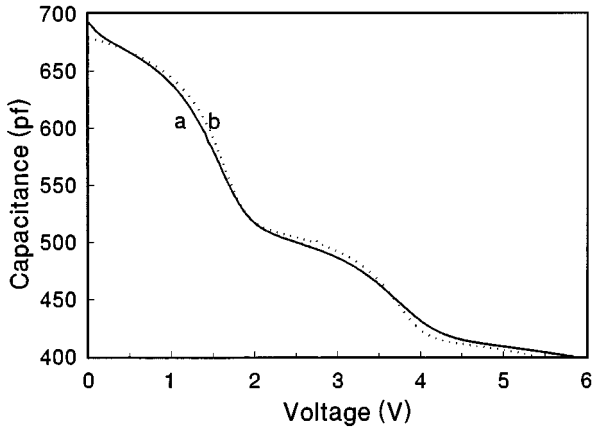

FIG. 11. The measured (a) and simulated (b) *C-V* curves for sample *E*.

V. RESULTS AND DISCUSSION

The measured *C-V* curve of sample *A*, containing a single quantum well with the structure of $Si(200\,nm)/Si_{0.67}Ge_{0.33}(15\ nm)/Si(300\ nm)/Si(100)$ is shown as curve *a* in Fig. 7. The doping concentrations in the Si barrier and SiGe well are 1×10^{16} and 4×10^{17} cm^{-3}, respectively, as confirmed by the secondary-ion-mass spectroscopic (SIMS) measurement (see Fig. 8). The computer-simulated *C-V* curve using the above parameters is shown as curve *b* in Fig. 7. The deviation between curves *b* and *a* is due to the effect of interfacial charge density. Curve *c* shows the calculated *C-V* characteristics by assuming an interfacial charge density of -1×10^{11} cm^{-2}. The existence of such negatively charged interfacial defects has been verified by the deep-level transient spectroscopic measurements.[10] From the capacitance value of the *C-V* plateau, the cap thickness L_c is estimated to be 200 nm, which is in agreement with the SIMS profile (Fig. 8). The band offset $\Delta E_V = 0.22$ eV derived from the simulation agrees well with the result measured by admittance spectroscopy.[11]

Figure 9 shows the comparison of the *C-V* curves for another two single-quantum-well samples (*B* and *C*). All structural parameters are the same except for the Ge content in the well. The difference between these two *C-V* curves is the plateau width. The sample with large well depth (larger Ge content) contains higher carrier concentration in the well. The applied bias voltage for depleting the carriers in the well must be higher than that in the sample with shallow well depth. The experimental results here are in coincidence with the theoretical analysis in Sec. IV.

Figure 10 illustrates the *C-V* carrier-concentration profiles of three different samples *B*, *C*, and *D* with the same structure but different Ce contents. The *p-x* relations there are obtained by differentiating the measured *C-V* curves according to Eqs. (12) and (13). The peak carrier concentration increases with the well depth, which is resulted by the carrier transfer from the barrier into the well. However, as mentioned in Sec. IV, Fig. 10 could not be treated as the real carrier-concentration profiles in the quantum-well samples.

The *C-V* measurements for multiple-quantum-well samples have also been performed. Figure 11 is the result of sample *E* with five quantum wells each, and has a well width

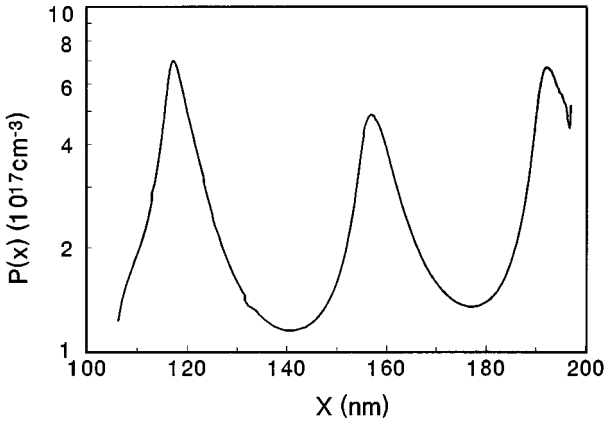

FIG. 12. The C-V carrier-concentration profile of sample E.

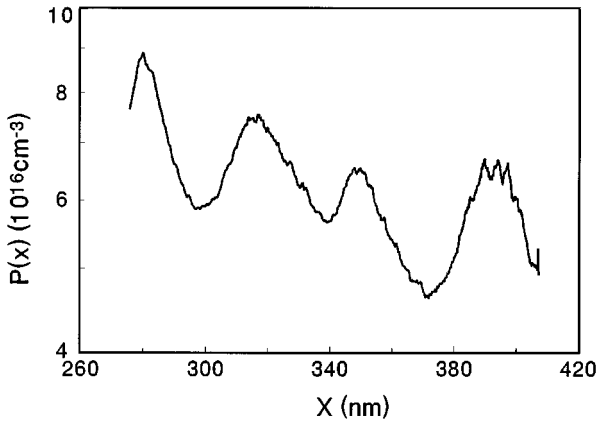

FIG. 14. The C-V carrier-concentration profile of sample F.

of 15 nm, a barrier width of 25 nm, and a Ge content of 0.33. The experimental result (curve a) shows three capacitance plateaus, each corresponds to the depletion of the carriers of a certain well. At high bias voltage, the very strong electric field in the cap layer causes the breakdown of the Schottky barrier. This limits the access of the last two wells in the C-V measurement. Curve b in Fig. 11 is the result of a theoretical simulation, which coincides very well with curve a.

Figure 12 is the C-V carrier-concentration profile obtained from Fig. 11. Although it does not represent the real carrier-concentration distribution, it can provide qualitatively more straightforward information than Fig. 11. First, the peaks in $p(x)$ curve correspond to the locations of the quantum wells. Second, the peak heights are related to the average carrier concentrations in the wells. Third, Fig. 12 is more sensitive to show the quantum-well structure than Fig. 11. The last point is especially clear for those narrower wells. Figure 13 shows the experimental (a) and theoretical (b) C-V curves of sample F containing multiple quantum wells with a well thickness of only 5 nm. Since the narrow well leads to the small plateau width in the C-V curve, it is difficult to identify the plateau structures in Fig. 13. By transferring the C-V curve into the $p(x)$ profile, the individual well structures could be clearly seen, as shown in Fig. 14.

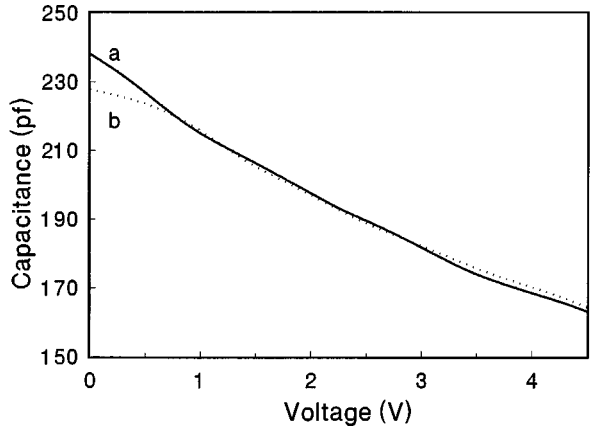

FIG. 13. The measured (a) and simulated (b) C-V curves for sample F.

By using the computer simulations of the C-V curves, the band offsets of our samples could be derived as shown in Table I. The values coincide fairly well with our admittance spectroscopy measurements, but are a little smaller than the theoretical prediction.[11]

VI. CONCLUSIONS

Based on numerically solving the Poisson equation for a Schottky junction containing $Si_{1-x}Ge_x$/Si single quantum well, the energy-band bending and the extension of space-charge region under the variation of bias voltage are elucidated. The C-V characteristics of the quantum-well structures are also calculated. The most prominent feature of the C-V curve which differs from that of the bulk semiconductors is the appearance of a capacitance plateau, which is caused by the pinning of the boundary of the space-charge region at the well boundary during the variation of the bias voltage by the high carrier concentration in the well. The experimental results coincide well with the theoretical prediction. From the measured C-V curve, the structural parameters of the sample could be extracted, such as the thickness of cap layer, the carrier concentrations in the cap and buffer layers, the location of the quantum well, and the interfacial charge density between the well and buffer. The C-V carrier concentration profile in the quantum well derived by differentiating the C-V curve does not coincide with the real carrier concentration distribution; only the peak height of the C-V carrier concentration profile is related with the average carrier concentration in the well. The theoretical analysis in this work is also valid for multiple-quantum-well samples, although only a limited number of quantum wells could be accessed in the experimental measurements due to the breakdown of space-charge region under high bias voltages.

ACKNOWLEDGMENTS

The authors wish to acknowledge Bo Zhang for data processing. This work was supported by the State Commission of Science and Technology of China.

[1] E. F. Schubert, R. F. Kopt, J. M. Kuo, H. S. Luftman, and P. A. Garbinski, Appl. Phys. Lett. **57**, 497 (1990).
[2] H. Kroemer, W. Y. Chien, J. S. Harris, Jr., and D. D. Edwall, Appl. Phys. Lett. **36**, 295 (1980).
[3] K. Tittelbach-Helmrich, Semicond. Sci. Technol. **8**, 1372 (1993).
[4] M. A. Rao, E. J. Caine, H. Kroemer, S. I. Long, and D. I. Babic, J. Appl. Phys. **61**, 643 (1987).
[5] J. C. Brighten, I. D. Hawkins, A. R. Peaker, E. H. C. Parker, and T. E. Whall, J. Appl. Phys. **74**, 1894 (1993).
[6] X. Letartre, D. Stievenard, and E. Barbier, J. Appl. Phys. **69**, 7912 (1991).
[7] X. Letartre, D. Stievenard, and E. Barbier, Appl. Phys. Lett. **58**, 1047 (1991).
[8] F. Lu, J. Jiang, H. Sun, D. Gong, and X. Wang, J. Appl. Phys. **75**, 2957 (1994).
[9] X. Letartre, D. Stievenard, M. Lannoo, and D. Lippens, J. Appl. Phys. **68**, 116 (1990).
[10] Q. H. Wang, F. Lu, D. W. Gong, J. B. Wang, H. H. Sun, and X. Wang, Phys. Rev. B **50**, 18 226 (1994).
[11] F. Lu, J. Jiang, H. Sun, D. Gong, X. Zhang, and X. Wang, Phys. Rev. B **51**, 4213 (1995).